PCCP

PAPER

View Article Online
View Journal | View Issue

Cite this: *Phys. Chem. Chem. Phys.*, 2015, **17**, 315

How morphology and surface crystal texture affect thermal stability of a metallic nanoparticle: the case of silver nanobelts and pentagonal silver nanowires

Ehsan Marzbanrad,[ab] Geoffrey Rivers,[b] Peng Peng,[ab] Boxin Zhao[ac] and Norman Y. Zhou*[ab]

Thermal instability of metallic nanoparticles is typically attributed to chemical attack by contaminants. However, thermodynamic stability is independent of other affecting parameters. The importance of this will be clarified when the structural change toward a more stable thermodynamic condition may be followed by a chemical reaction with the surroundings, which may cause a wrong diagnosis. In this research, molecular dynamics simulations and experimental observations were performed to investigate the effect of crystallography and surface texture on stability at high temperature using two closely related model nanoparticles: silver nanobelts and pentagonal nanowires. Previously, the instability of silver nanowires was associated with sulfidation of the wire at high temperature. However, we found that the silver nanowires are inherently unstable at high temperature, degrading due to the high-energy nature of the nanowire's predominately (100) crystallographic surface and pentagonal geometry. In contrast, the silver nanobelts resist thermal degradation up to 500 °C because of their predominately low-energy (111) crystallographic surfaces. In this case study, we successfully demonstrate that inherent thermodynamic stability driven by morphology is significant in metallic nanoparticles, and should be investigated when selecting a nanoparticle for high temperature applications. Moreover, we identify a new one-dimensional nanoparticle, the silver nanobelt, with inherent high-temperature stability.

Received 15th September 2014,
Accepted 31st October 2014

DOI: 10.1039/c4cp04129a

www.rsc.org/pccp

Published on 31 October 2014. Downloaded on 27/02/2015 20:24:12.

1. Introduction

The thermal stability of crystalline metallic nanoparticles is a challenging topic in nanoscience, which can limit the employment of a nanoparticle at high temperature.[1–8] This is a complicated issue, since processes of chemical attack, diffusion, and phase change are all temperature dependent, and so it is often difficult to identify which are the dominant causes of thermal instability in a particular case. It has been shown that for metallic nanoparticles smaller than 2 nm the surface atoms play a critical role.[1] In this regime, most of the atoms are at the surface, and the arrangement of the atoms influences the stability of the particles independent of other factors. Researchers have employed protective layers to manipulate the surface atoms and enhance the stability of the nanoparticles within this size regime.[1,2] At larger particle size regimes between 2 nm and 100 nm, the internal bulk of the particle becomes sufficient to produce a transition between the surface and core atoms. In this size regime, systematic investigation of thermal stability of metallic nanoparticles has been limited, though nanoparticles of this size are employed in many applications. In this size regime, research typically investigates the contribution of surface texture to stability in terms of how easily the nanoparticle surface is chemically attacked by outside contaminants. However, there remains an open question as to whether crystallography and surface texture act independently on the thermal stability of these metallic nanoparticles. In other words, before referring to the effect of external reactants, it is worthwhile to answer whether a nanoparticle is thermodynamically stable at high temperature or exhibits sufficient kinetic barriers to resist changing to a more stable form.

Of the metallic nanoparticles, silver is a desirable nanomaterial thanks to its remarkable physical and chemical properties. Researchers are developing silver nanoparticles for many unique applications,[9–20] synthesizing them in a variety of sizes and morphologies during the last two decades.[21–24] Among those reported, the pentagonal silver nanowire is unique: a high aspect-ratio particle, achieving excellent electrical conductivity

[a] *Centre for Advanced Materials Joining, University of Waterloo, Waterloo, Canada. E-mail: nzhou@uwaterloo.ca*
[b] *Department of Mechanical and Mechatronics Engineering, University of Waterloo, Waterloo, Canada*
[c] *Department of Chemical Engineering, University of Waterloo, Waterloo, Canada*

Published on 31 October 2014. Downloaded on 27/02/2015 20:24:12.

and mechanical strength.[25,26] These desirable properties have led to many previous studies where silver nanowires were employed for various applications such as flexible and transparent electronics, nanosensors, transparent heaters, and nanocomposites.[27–31] However, it has been reported that these silver nanowires are not stable when subjected to high temperatures.[6,27,32,33] This has been attributed to sulfidation of silver nanowires, based on energy dispersive spectroscopy analysis.[32,34,35] Sulfidation of silver is a well-known process that can happen at room temperature and is intensified at elevated temperatures. Therefore sulfidation can be one of the driving forces of degradation of silver nanowires, under an appropriate environment. However, it is not clear how temperatures alone contribute to this instability, which could be investigated by annealing under vacuum or in an inert atmosphere. This is of concern because this instability may also be driven by the physical properties of nanoparticles such as surface crystallography. Such an effect would confound research efforts to mitigate the thermal instability of silver nanoparticles intended for high temperature applications; techniques that prevent chemical attacks would be undermined or obscured by any intrinsic thermodynamic instabilities that exist for that particle crystallography.

It is well known that different crystal planes have different packing densities; more packing means lower energy and higher stability. In the case of silver, the close-packed (111) plane is the lowest energy crystal plane with maximum packing, and therefore the most stable. By comparison, the (100) plane is more loosely packed, has higher energy, and is therefore relatively unstable. However, no work has been reported to utilize theoretical calculation or experimental observation to investigate the surface morphology effects on thermal instability for nanoparticles such as nanowires. Silver nanowires have a pentagonal cross-section when viewed perpendicular to their major axis, with each edge corresponding to a (100) surface that runs parallel to the major axis. The pointed tips of the nanowires, which project in the direction of the major axis, are five-sided pyramids where each triangular face is a (111) surface. It means that this crystal morphology, which is mainly covered by the five high-energy 100 planes, is not the most stable possible configuration for a silver nanoparticle in theory.

Recently we synthesized a new one-dimensional flat silver nanoparticle, the nanobelt,[36] by simultaneous self-assembly and nanojoining of hexagonal and triangular silver nanoplates as structural blocks. The nanoplates have been previously investigated[37–40] and their crystal structure, explored by Elechiguerra *et al.*,[35] were found to have a twin plane at the center and two (111) planes on the flat surfaces.[24] The majority of the nanobelt surface area is composed of closed packed (111) planes, as a result of realignment of the nanoplates during joining.[36] Therefore, it could be expected that silver nanobelts should be stable at higher temperature than pentagonal silver nanowires.

In this research, we demonstrate how the morphology and surface texture of a nanoparticle can affect its thermodynamic instability and how this inherent instability is temperature dependent. This question is answered by comparing the thermal stability behavior of two closely-related metallic nanoparticles, which differ mainly in surface crystal texture: silver nanowires and silver nanobelts. To do this research, we employed MD simulation and experimental observation to compare the thermal stability of these nanoparticles. Moreover, this study clarified the thermal stability of silver nanowires and nanobelts, which indicated that nanobelts are a new candidate for high temperature applications, such as a transparent heater material.

2. Results and discussion

2.1. MD simulation of silver nanowires

The results of four MD simulations of a short silver nanowire being annealed at four different temperatures (−272 °C, 200 °C, 300 °C, and 400 °C) are presented in Fig. 1. It is apparent that the nanowire is thermally unstable above 200 °C, with degradation worsening as temperature increases. The −272 °C simulation (Fig. 1a) reveals the nanowire to be stable and well ordered, having developed no apparent defects; the (100) plane of the nanowire side is highlighted in the inset view. At 200 °C (Fig. 1b) and above (Fig. 1c to d), atoms (arrows 1, 3, 6 and 7) migrate from their initial positions onto (100) surfaces to form

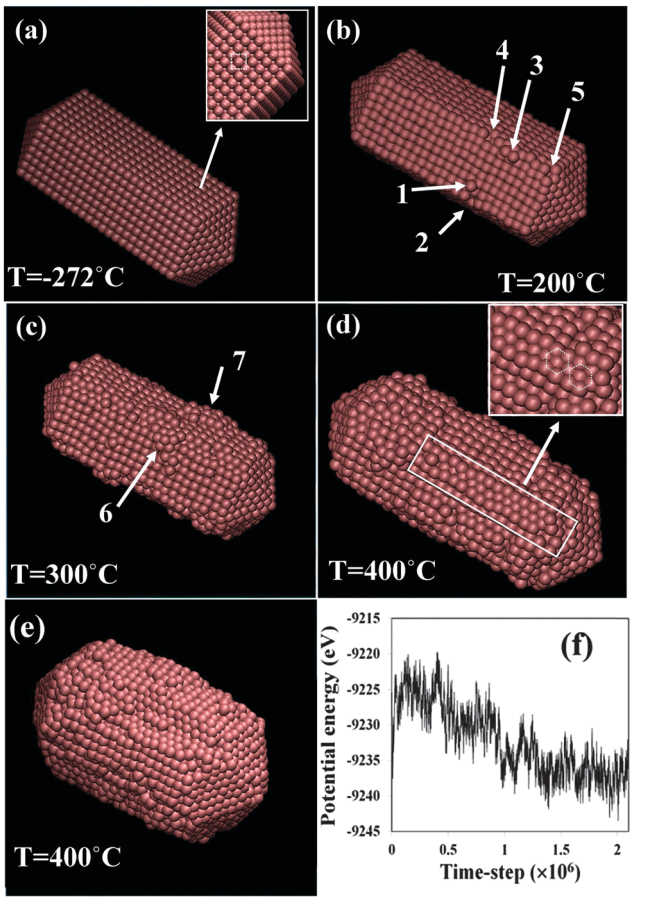

Fig. 1 (a) Structure of silver nanowires annealed at −272 °C; (b) silver nanowire annealed at 200 °C; (c) silver nanowire annealed at 300 °C; (d) silver nanowire annealed at 400 °C; (e) a larger silver nanowire annealed at 400 °C for 2 × 10^6 time-steps, twice as long as the previous cases; (f) potential energy change of the silver nanowire during annealing at 400 °C.

This journal is © the Owner Societies 2015

Published on 31 October 2014. Downloaded on 27/02/2015 20:24:12.

clusters (arrows 3, 6 and 7), leaving vacancies at the edges where the (100) surfaces intersect (arrows 2, 4 and 5). In the 400 °C simulation (Fig. 1d), a great deal of degradation has occurred; large clusters of migrated atoms have formed, and the edges at the intersection of the (100) surfaces have eroded. These eroded edges leave behind a new surface crystallography: the hexagonal close-packed (111) crystal plane, outlined by the white rectangle in (Fig. 1d) and shown magnified in the inset. Interestingly, the tips of the nanowire were stable at each of these simulated temperatures, and are composed exclusively of (111) crystal planes. An additional simulation of a larger diameter nanowire at 400 °C for 2×10^6 time-steps is also included (Fig. 1e), which confirms that the larger nanowire degrades in the same way as the smaller one. The longer simulation time in this case reveals that the degradation is not limited to a single atomic layer at the sharp edge: the nanowire will continue to degrade, eroding (100) surfaces while producing surface clusters and new (111) planes.

These qualitative observations imply that the thermal instability of silver nanowires is primarily a result of surface atoms diffusing from the edges of high-energy (100) planes to form new surfaces. The production of (111) surfaces, and the lack of observed degradation of the nanowire tips, shows that the (111) surfaces are significantly more stable than the (100) planes. Fig. 1f presents the potential energy of the nanowire as the 400 °C simulation progressed; as anticipated, there is a reduction of potential energy as the nanowire degrades.

Fig. 2 is an analysis of the potential energy, kinetic energy, and displacement of atoms for a simulated nanowire at 200 °C. This data is gathered from the beginning of the simulation, using the atomic states at five equally spaced time steps between 10 000 and 11 000. The nanowire tips are stable at all temperatures, and so it is reasonable to remove them from the following analysis. Coordinates were assigned by projecting the initial position of each atom onto an X–Y plane perpendicular to the major axis of the central nanowire segment. Fig. 2a shows atoms plotted by the A–J parameter *versus* the initial X–Y coordinate; surface, interior, and twin boundary atoms are clearly distinguished. The remaining properties of Fig. 2 are plotted with respect to the radial distance (R) from the central Z-axis, calculated by eqn (1).

$$R = \sqrt{X^2 + Y^2} \tag{1}$$

where X and Y are the instantaneous coordinates of the atoms projected onto the X–Y plane. To highlight that simulated atom states are not being over-constrained, Fig. 2b–d displays the state of every atom for each distance R, rather than presenting average values. Fig. 2b demonstrates that interior and twin boundary atoms have similar potential energy, while the surface atoms have notably higher energy, implying that the instability is likely not the result of the twin boundary presence. The highest potential energies belong to the surface atoms farthest from the center axis, and therefore located close to the edges that describe the intersections of the (100) surfaces. Fig. 2c presents the kinetic energy with respect to radial distance, demonstrating that the simulation was appropriately isothermal. Plotting atom displacement in a similar manner (Fig. 2d), we see that the highest mobility was displayed by members of the edge-occupying group of surface atoms.

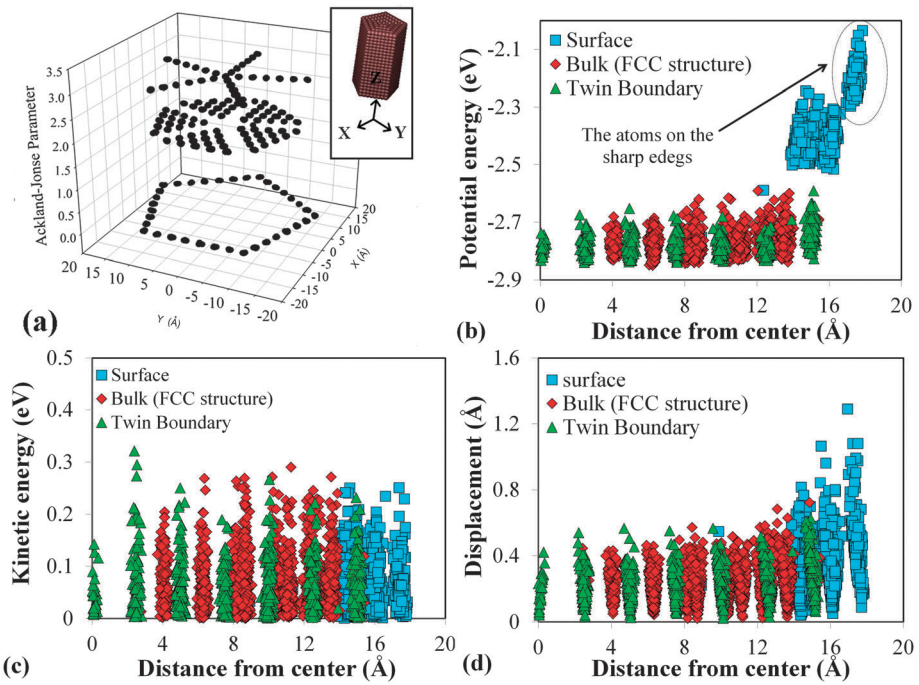

Fig. 2 (a) The Ackland–Jones parameter of the atoms of the silver nanowire *versus* x and y dimension of the atoms; (b) potential energy of the atoms *versus* distance from the center of the cross section (R); (c) kinetic energy of the atoms *versus* distance from the center of the cross section (R); (d) displacement of atoms *versus* distance from the center of the cross section (R).

Published on 31 October 2014. Downloaded on 27/02/2015 20:24:12.

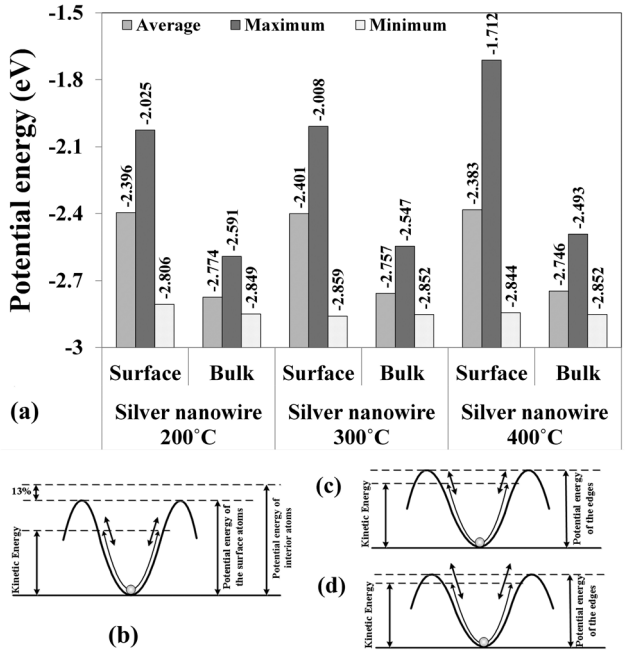

Fig. 3 (a) Average, maximum and minimum potential energy of the surface and interior atoms at 200 °C, 300 °C and 400 °C; (b) schematic graph shows the kinetic energy and vibration of a surface atom compared to its potential energy; (c) schematic graph shows the kinetic energy and vibration of an edge atom compared to potential energy at low temperature; (d) schematic graph shows the kinetic energy and vibration of an edge atom compared to potential energy at high temperature.

To explain how temperature can affect degradation, the potential energy of surface and interior atoms after annealing at 200 °C, 300 °C and 400 °C were compared (Fig. 3a). The average potential energy of the surface is around 13% lower than the interior at these temperatures in all cases. However, considerable differences can be observed in the maximum potential energy of surface atoms. In other words, the maximum potential energy of a small fraction of the atoms is very high, which may allow them to escape from their original position. Based on this data, the mechanism of the instability of surface atoms can be explained considering Fig. 3b though d. Fig. 3b shows the kinetic energy and vibration of the surface atoms in their potential well. The arrows in this figure show fluctuation of the kinetic energy. MD simulation data reveal that the interior atoms are stable and their vibration is not enough to let the atoms escape from the potential well. The potential energy of surface atoms is around 13% higher than the interior atoms (Fig. 3b). When the temperature is lower than 200 °C, the atoms of the corners remain in the potential energy well (Fig. 3c). However, increasing temperature to 200 °C or more will provide enough kinetic energy for some of the atoms to escape from their potential well (Fig. 3d). Obviously, few atoms with high kinetic energy have this chance to move out of their position. When an atom moves out from its position, the potential energy of the atoms around its vacancy increases, they will be more susceptible to escape from their original position, and this process can continue.

2.2. Experimental annealing of silver nanowires

The thermal stability of silver nanowires was examined experimentally through SEM and EDX of the annealed samples under an argon atmosphere at 200 °C and 300 °C. Before annealing, Fig. 4a shows silver nanowires featuring sharp edges and well-defined

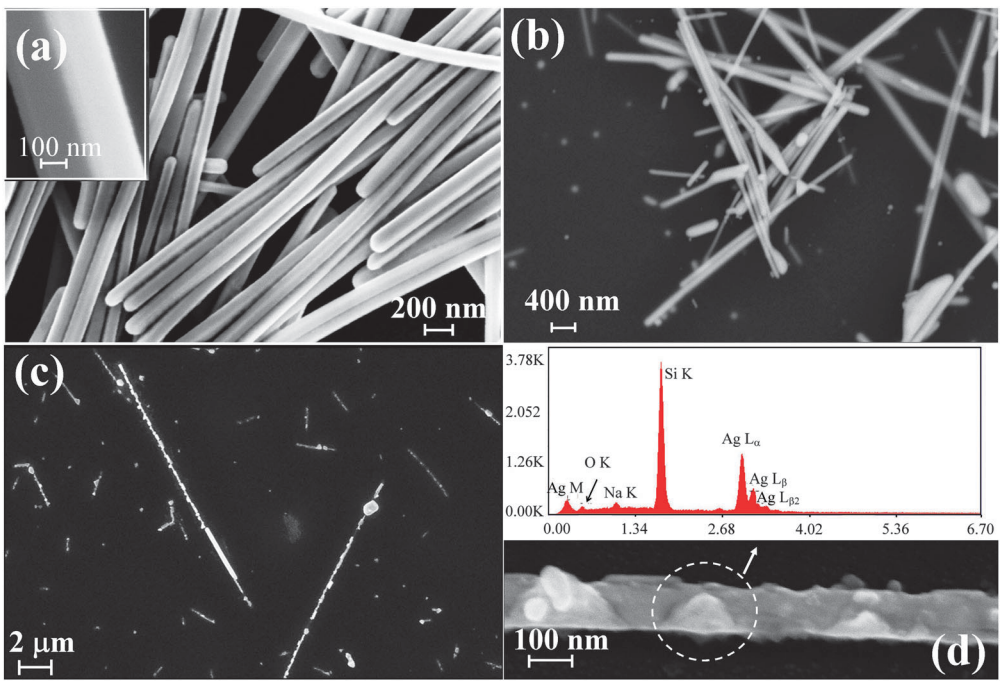

Fig. 4 (a) Synthesized silver nanowires; (b) silver nanowires after annealing at 200 °C for 100 h; (c) silver nanowires after annealing at 300 °C for 10 h; (d) high magnification image of a silver nanowire after 10 h of annealing at 300 °C, inset: the EDX analysis of the highlighted area.

 This journal is © the Owner Societies 2015

Published on 31 October 2014. Downloaded on 27/02/2015 20:24:12.

morphology. Similarly, silver nanowires annealed for 10 hours at 200 °C are found to be largely stable, having maintained their gross morphology, as shown in Fig. 4b. However, after annealing for 10 hours at 300 °C (Fig. 4c) the nanowires were clearly unstable, having degraded by eroding in some areas while growing new surface features in others; this degradation is easily visible at high-magnification (Fig. 4d). The degradation is not electrochemical in nature; inset is EDX spectra of the indicated area, confirming that no contaminants were present, including sulfur. This contradicts the current literature findings that the sulfidation of silver nanowires is the cause of their thermal instability, and instead reveals that silver nanowires are inherently unstable at high temperature.

For silver nanowires, the MD simulations and experimental observations indicate inherent thermal instability above 200 °C, which makes them unsuitable for high temperature applications. The results imply that the greatest factor in this is the high potential energy of the nanowire surfaces, due to the majority of them featuring (100) crystallography. In comparison, the (111) planes of the surfaces at the tips of the nanowires appeared stable in the MD simulations, owing to their low-energy close-packed state. If this analysis of silver nanowires is correct, it follows that the primary feature of a silver nanoparticle with higher thermal stability would be a majority of surfaces composed of more stable (111) planes.

2.3. MD simulation of silver nanobelts

Recently, we have synthesized silver nanobelts, a new high-aspect ratio silver nanoparticle featuring (111) crystallography on its broadest flat surfaces. These nanobelts are produced easily through the nanojoining of hexagonal and triangular structural blocks.[36] If the nanobelts were found to be more thermally stable than silver nanowires, they would not only support the hypothesis of the cause of nanowire degradation, they would also provide a feasible alternative to silver nanowires for high temperature applications.

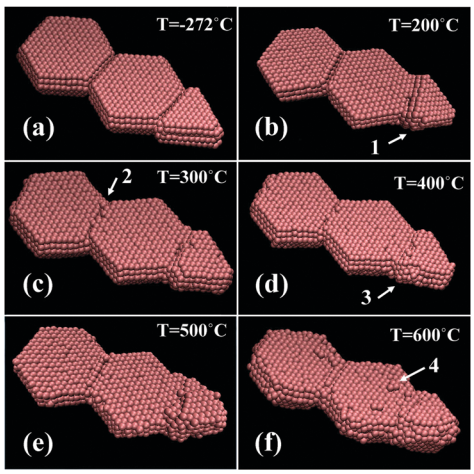

Fig. 5 (a) Structure of a silver nanobelt annealed at −272 °C; (b) silver nanobelt annealed at 200 °C; (c) silver nanobelt annealed at 300 °C; (d) silver nanobelt annealed at 400 °C; (e) silver nanobelt annealed at 500 °C; (f) silver nanobelt annealed at 600 °C.

Six MD simulations of a short segment of a silver nanobelt annealed at different temperatures (−272 °C, 200 °C, 300 °C, 400 °C, 500 °C, and 600 °C) are presented in Fig. 5. The final states of these simulations demonstrate that the nanobelt is thermally stable in temperatures up to and including 500 °C (Fig. 5a to e). The −272 °C simulation (Fig. 5a) reveals the nanobelt to be well ordered, having developed no apparent defects. From 200 °C and above, the nanobelt sub-units undergo a small relative rotation at their junctions (arrow 1) to minimize internal stresses. From 300 °C to 500 °C (Fig. 5c–e) the nanobelt develops sparse surface vacancies along its edges. Instead of forming random surface clusters like those on the nanowires, the migrated atoms relocate to the seams between the sub-units (arrow 2), filling the joints between the nanobelt sub-units and improving continuity of the (111) surface. At ass high as 400 °C and 500 °C (Fig. 5d and e) the simulations demonstrate that the broad (111) surfaces of the nanobelt are still intact. However, the minor restructuring of the sharp edges occurs (arrow 3). In the 600 °C simulation (Fig. 5f) the nanobelt displays thermal instability, with atoms migrating from the edges to form clusters on the flat (111) surfaces (arrow 4). At this temperature, it is expected that atoms would continue to migrate across the surface until the nanobelt morphology is completely degraded.

Numerical analysis of these MD simulation results (Fig. 6) evaluates the potential energy, kinetic energy, and displacement of atoms in the 200 °C simulation, using the long-axis of

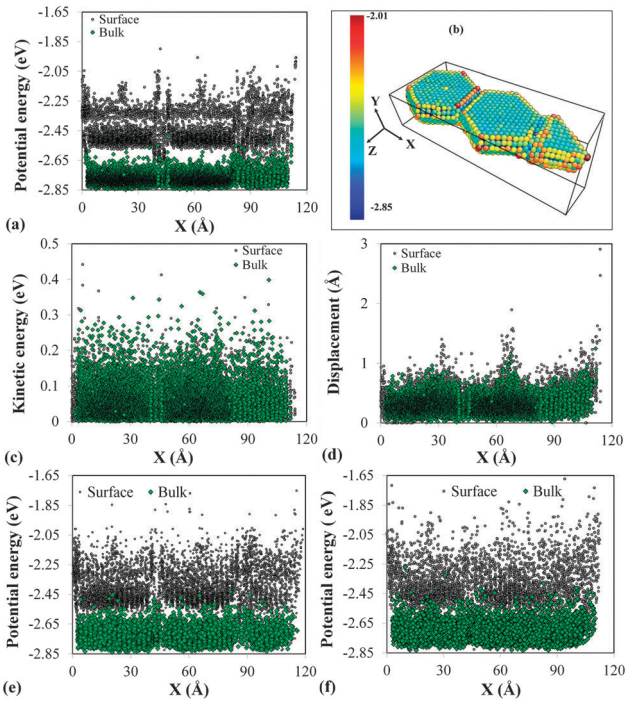

Fig. 6 (a) Potential energy of atoms at 200 °C *versus* position of the atom on the *X* axis; (b) silver nanobelt, the color of atoms shows their potential energy; (c) kinetic energy of atoms at 200 °C *versus* position of atom on the *X* axis; (d) displacement of atoms at 200 °C; (e) potential energy of atoms at 500 °C; (f) potential energy of atoms at 600 °C.

Published on 31 October 2014. Downloaded on 27/02/2015 20:24:12.

the simulated nanobelt segment as the *X*-axis. Similar to the previous analysis, this data was gathered from the beginning of the simulation using the atomic states at five equally spaced time steps between 10 000 and 11 000, and the surface and interior atoms were differentiated using the Ackland–Jones parameter. Interestingly, Fig. 6a shows that the surface atoms are divided into two distinct energy bands across the entire nanobelt length. A color-coded 3D model of the nanobelt (Fig. 6b), with each atom colored according to its potential energy, confirms that the broad and flat (111) surfaces of the nanobelt have lower energy than the edges, and that the high-energy atoms are a small fraction of the total nanoparticle. Some of the small faces are high-energy, as seen on the visible side of the triangular sub-unit; close inspection reveals that these are composed of the minority (100) surface crystallography. A comparison between the nanobelt and nanowire (Fig. 6 and 2, respectively) demonstrates that even at the edges of the nanobelt, the potential energy of surface atoms is smaller than nanowires. The only exceptions to this are few atoms at the sharp vertexes of the nanobelt, which Fig. 5 showed were not sufficient to produce thermal instability. The kinetic energy of surface and interior atoms have no significant difference (Fig. 6c), while surface atoms at the boundary and the corners are high mobility atoms based on the displacement of atoms (Fig. 6d).

The initial potential energies of atoms in the 500 °C and 600 °C simulations are plotted in Fig. 6e and f. As expected, the 500 °C simulation (Fig. 6e) has a pattern of potential energies approximately similar to that of the 200 °C (Fig. 6a). The lower surface energy band at 500 °C displays nearly the same as 200 °C. However, the band corresponding to the higher-energy edge atoms shows more high-energy atoms. In contrast, the 600 °C simulation (Fig. 6f) reveals that the surface atoms occupy a diffuse distribution, and represent the onset of thermal instability of silver nanobelts in the vicinity of 600 °C.

2.4. Experimental annealing of silver nanowires

Similar to the investigation of nanowires, we compare these MD simulations to SEM observations of silver nanobelts, first in their as-synthesized state, and then after annealing at various temperatures. Since these nanobelts are newly developed, we also include X-ray diffraction (XRD) and TEM observations to better demonstrate their nature. Before annealing, Fig. 7 demonstrates the as-synthesized condition of the nanobelts. A low-magnification SEM image (Fig. 7a) shows many high-aspect ratio nanobelts, inset with a higher magnification example of a serpentine nanobelt. SEM of several stacked nanobelts in Fig. 7b reveals the thickness of each belt to be in the range of 20 nm to 30 nm, and imaging by TEM (Fig. 7c) demonstrates that the belt is composed of joined nanoplates. The inset diffraction pattern of the indicated area of Fig. 7c confirms that the broad nanobelt surfaces are composed of (111) crystallography. XRD of the as-synthesized nanobelts (Fig. 7d) confirms this further, presenting only one peak corresponding to the (111) plane (in accordance with JCPDS card number 00-001-1164). The corresponding XRD on synthesized nanobelt powder reveals this structure to be

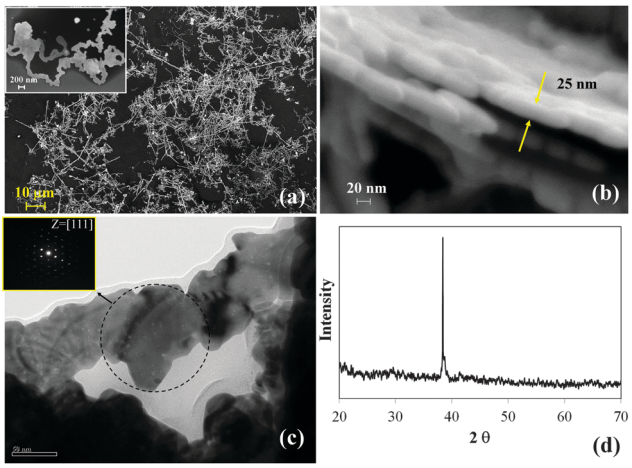

Fig. 7 (a) Synthesized silver nanobelts. The added image shows a single silver nanobelt; (b) thickness of silver nanobelts; (c) TEM image of a silver nanobelt, the added images show the selected area diffraction pattern of the marked area; (d) X-ray diffraction pattern of the synthesized silver nanobelts.

uniform, and all nanobelts to share this (111) broad surface. This combined characterization confirms that the model nanobelt segment in the MD simulation is a good representative of the as-synthesized material.

Fig. 8 shows SEM images of five batches of nanobelts, each annealed at a different temperature for 10 hours. After annealing at 200 °C, Fig. 8a reveals that the nanobelts remained

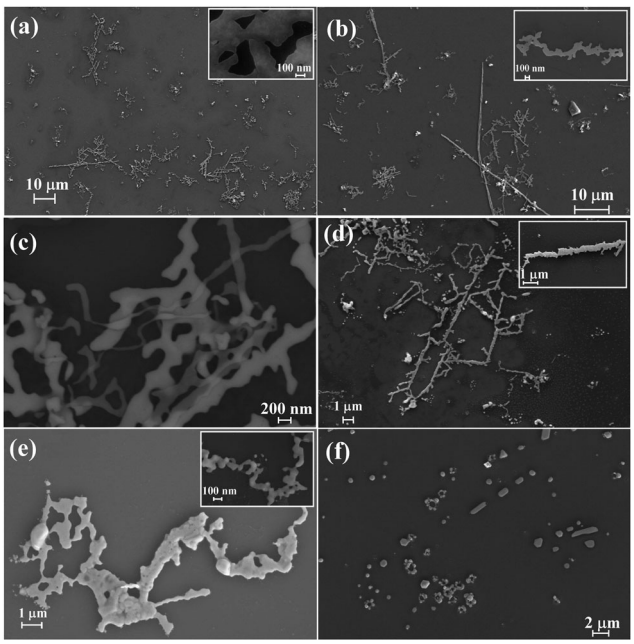

Fig. 8 (a) Silver nanobelts after 10 hours of annealing at 200 °C; (b) silver nanobelts after 10 hours of annealing at 300 °C; (c) agglomerated silver nanobelts after 10 hours of annealing at 300 °C are stable and do not sinter; (d) silver nanobelts after 10 hours of annealing at 400 °C; (e) silver nanobelts after 10 hours of annealing at 500 °C; (f) silver nanobelts after 10 hours of annealing at 600 °C.

This journal is © the Owner Societies 2015

Published on 31 October 2014. Downloaded on 27/02/2015 20:24:12.

stable, as predicted by the MD simulation. Inset is a high magnification view, demonstrating that the surface and edges of the nanobelts are intact. It is worthwhile to mention that the PMAA that covers the surface of the nanobelts will degrade at around 150 °C;[41] therefore, it cannot affect our stability observations. Similar to 200 °C, after annealing at 300 °C, the nanobelts remained stable (Fig. 8b), and did not sinter to one another (Fig. 8c). The nanobelts remain stable enough to maintain their high-aspect ratio form when annealed at temperatures of 400 °C and 500 °C (Fig. 8d and e). Insets show that the edges are still intact at 400 °C (Fig. 8d), but after exposure to 500 °C the edges erode and contacting nanobelts begin to sinter together (Fig. 8e), although the belts maintain their one-dimensionality. After 10 hours of annealing at 600 °C (Fig. 8f), the nanobelts are found to be thermally unstable, and have lost their high-aspect ratio morphology due to the continuing diffusion of atoms at high temperature, as predicted by the simulations.

XRD patterns of the annealed nanobelts at different temperatures are presented in Fig. 9a. These XRD patterns reveal that the crystal structure of the nanobelts did not change after annealing at the 200 °C, 300 °C, and 400 °C. At 500 °C, there are two very small peaks belonging to (200) and (220) planes of the silver crystal (indicated by arrows on the Fig. 9a). Fig. 9b shows an SEM of a nanobelt after annealing at 500 °C, and Fig. 9c presents EDX analysis of the circled area of Fig. 9b. Combined, these findings confirm that this sample was not corroded by sulfur, and that the small structural change observed by XRD is because of sintering and changes in the morphology of the particles. The XRD pattern of the annealed sample at 600 °C has a completely different crystal structure, confirming that degradation occurred at this temperature. This is in agreement with MD simulation and SEM images of the sample after annealing at this temperature (Fig. 5f and 8f).

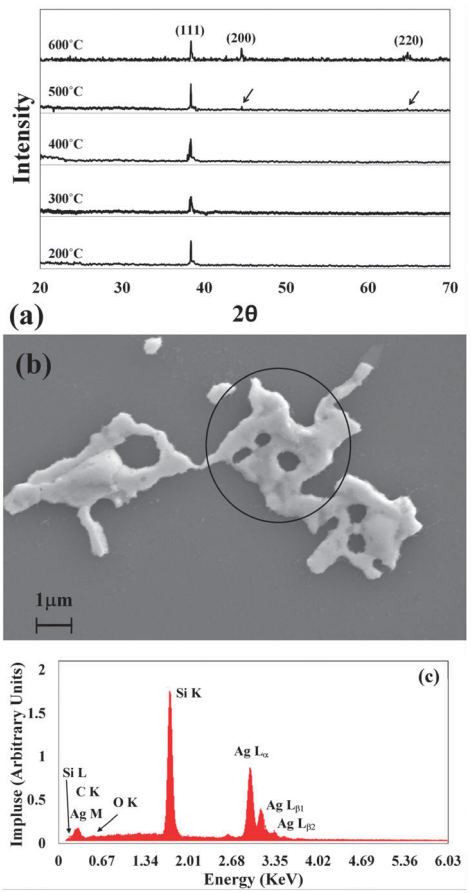

Fig. 9 (a) XRD pattern of the annealed samples at 200 °C, 300 °C, 400 °C, 500 °C and 600 °C; (b) SEM of the annealed sample at 500 °C; (c) EDX analysis of the marked area of the SEM image (b).

3. Conclusion

We have demonstrated the importance of morphology and surface atomic arrangement as an independent influence on the thermal stability of metallic nanoparticles in the 2–100 nm size regime. This is a fundamental issue, which should be addressed first when studying a nanoparticle at high temperature, which has not been previously addressed by the literature. To do this research we performed comparative studies of silver nanowires and silver nanobelts by both MD simulation and experimental observation. These particles are excellent candidates for this study because both are one-dimensional and their lengths are in the same range, while their crystal textures are completely different. For pentagonal silver nanowires, the MD simulations and experimental observations indicate inherent thermal instability due to most surfaces featuring (100) crystallography. This instability results in the erosion and diffusion of atoms across the surface, followed by their recrystallization as new clusters. The greatest erosion of these surfaces appears to occur at the edges between two adjoining (100) surface. This is likely in part due to the geometry of the cross section placing the atoms in proximity to two high-energy surfaces. Through this process, the nanowires appear to favor the formation of new surfaces with (111) crystallography, and the obstruction of (100) planes by the recrystallizing clusters. All of this has been observed without detectable contaminants, demonstrating that this degradation is independent of chemical attack. In contrast to silver nanowires, the MD simulations and experimental observations indicate that silver nanobelts are stable up to 600 °C, which makes them suitable for high-temperature functional materials. These results showed that the broad and flat (111) surfaces of the nanobelts were highly resistant to the effects of high temperature, which supports the prior statement that low energy crystal planes with high packing density provide better thermal stability.

This case study clarifies that the surface texture of a nanoparticle plays a key role in stability. Based on the presented results, increasing temperature provides enough energy for the surface atoms to displace and degrade the nanoparticle, independent of other contributors. This thermodynamic inherent instability is a fundamental issue and must be considered when selecting nanoparticle for high temperature applications. In the case of silver nanowires, sulfidation has been investigated as the cause of thermal instability before this research. However, this

Published on 31 October 2014. Downloaded on 27/02/2015 20:24:12.

research demonstrates that pentagonal silver nanowires are inherently unstable because of their high energy structure, and will degrade even in a non-corrosive atmosphere. Therefore, although sulfidation is a factor to be investigated, it is accompanied by an inherent thermodynamic instability that limits the performance of silver nanowires in high-temperature applications. In contrast, silver nanobelts are demonstrated to be high thermal stability one-dimensional silver nanoparticles, which might be feasible and high performance candidates for different nanotechnology applications. In addition, the intrinsic stability of silver nanobelts promotes them as a model nanoparticle for further research into the mitigation of degradation by chemical attack.

4. Simulation and experimental methods

4.1. MD Simulation

The calculations for MD simulation were performed using a C++ program developed by the authors, the results of which were visualized using visual molecular dynamics (VMD) and Atomeye.[42,43] The embedded atom method (EAM potential) is used for this simulation.[44,45] In EAM, the total energy is defined by eqn (2).

$$E_{\text{total}} = \sum_i F(\rho_i) + \frac{1}{2}\sum_{i,j,i\neq j} \phi_{i,j}(r_{ij}) \quad (2)$$

In which, ϕ_{ij} is the pair potential between two atoms i and j, which is a function of their distance r_{ij}. $F(\rho_i)$ is the energy required to embed atom i into the electronic gas due to all neighbor atoms, calculated by eqn (3):

$$\rho_i = \sum_{i\neq j} f(r_{ij}) \quad (3)$$

where $f(r_{ij})$ is the electron density contributed by atom j. The interatomic potential parameters of silver for EAM have been calculated and reported.[45] For this study, MD simulations were carried out in the canonical (*NVT*) ensemble. Temperature was kept constant during simulation according to the Nose–Hoover thermostat,[46,47] and equations of motion were solved numerically using the Verlet algorithm.[48] Cut-off radius in this MD simulation was set to 12 Å, and the time-step was one femtosecond.

For each atom, the potential energy is calculated by summing the bonding energy between that atom and its neighbors, and the total potential energy of the system was the sum of the potential energy of all atoms. Similarly, for each atom, the kinetic energy calculated according to the velocity of that atom, and the total kinetic energy of the system was the sum of the kinetic energy of all atoms. The displacement of each atom is calculated as the distance from its original position. To investigate the position of the atoms in the nanoparticle, the Ackland–Jones parameter was used to categorize the atoms based on their local crystal structure, setting a characteristic value for each atom.[49] In this MD simulation program, fcc structure was denoted by 2, hcp structure by 3 and unknown structure, such as a surface, by 1.

The simulated nanowire contained 3530 atoms, with the initial state designed according to the crystal structure of nanowires.[24] To show the effect of nanowire size on thermal stability, we did simulation by a nanowire containing 6355 atoms. The diameter of this wire was 6.2 nm, which was approximately two times larger than the first nanowire. The simulated nanobelt segment contained 4804 atoms, and was composed of three joined sub-units: two hexagonal nanoplates and one triangular nanoplate. To represent a real silver nanobelt accurately, the simulated nanobelt segment was constructed by initially placing the simulated nanoplates in a MD simulation domain at 300 K, with the distance between the nanoplates less than the cut-off radius of the MD program. Under these conditions, the surface atoms of the particles attracted each other, and the nanoplates joined to produce the model nanobelt segment. This joining mechanism was investigated by the author, and reported in our previous paper.[36] Using these simulated structures, thermal stability was studied by simulating the MD simulations at various desired temperatures for 10^6 time-steps in all cases.

4.2. Experimental procedure

The silver nanowires were prepared in a polyol solution with polyvinylpyrrolidone (PVP) as a structure-directing reagent, using a method modified from the literature.[50–53] In this study, 330 mg PVP ($(C_6H_9NO)_n$, K25, M_W = 24 000, Alfa Aesar) and 12.5 mg silver chloride (AgCl, Alfa Aesar) were mixed with 40 ml ethylene glycol (EG, Fisher Chemical) in a round-bottom flask to make solution A. This solution was heated to a temperature between 160 °C and 170 °C. Then, 110 mg silver nitrate was dissolved in 10 ml ethylene glycol liquid to form solution B. This solution was added into the solution A while stirring vigorously and the reaction conditions were continued for 4 hours. Silver nanowires were washed with deionized (DI) water to remove the residual ethylene glycol and PVP.

To synthesize a silver nanobelt, 2.1 g of silver nitrate ($AgNO_3$, Sigma-Aldrich) was added to 60 ml H_2O and agitated by ultrasonic bath for one minute to form $AgNO_3$ solution. Reducing solution was prepared separately by adding 0.68 g ascorbic acid (Alfa Aesar) and 0.16 ml poly (methacrylic acid, sodium salt) 40% in water (PMAA) solution (Aldrich Chemistry) as a structure-directing reagent to 200 ml H_2O and agitated by ultrasonic bath for one minute. Synthesis was performed by mixing these solutions while the mixture was stirred by a magnetic stirrer.

4.3. SEM, TEM and XRD characterization

SEM and TEM were utilized to investigate the morphology and crystallography of both nanoparticles and EDX was employed to analyze the chemical composition of the products. To prepare SEM, EDX and TEM samples, 0.5 ml of the suspension containing nanowires or nanobelts was added to 3 ml H_2O, then agitated by ultrasonic bath for 5 min. For SEM samples, 0.02 ml was deposited by pipette onto a clean silicon wafer, then dried under argon at 70 °C using a controlled atmosphere tube furnace. Immediately after drying, the samples were annealed at the

 This journal is © the Owner Societies 2015

Published on 31 October 2014. Downloaded on 27/02/2015 20:24:12.

proper temperature in the same furnace under an argon atmosphere. After annealing, the annealed samples were placed in a vacuum desiccator. For TEM samples, approximately 100 μl of the diluted suspension was deposited onto a TEM grid, then dried under room conditions.

XRD was utilized to characterize the crystal structure of the newly developed silver nanobelts. To prepare XRD samples without annealing, suspended nanobelts were collected on a filter paper (Whatman® # 1001042) by vacuum filtration to form a 1.2 mm thick film. This was dried at 70 °C in the air, then detached by peeling away the filter paper. To prepare all annealed XRD samples, 500 mg of silver nanobelts was dispersed in 10 cc water by ultrasonic agitation. This suspension was deposited onto an iron sheet (15 cm × 2.5 cm) drop-wise and dried under argon at 60 °C using a controlled atmosphere tube furnace, and then annealed. After annealing, the nanobelts were dispersed again in water using ultrasonic agitation, and then collected on a filter paper (Whatman® # 1001042) by vacuum filtration. This was dried under argon at 70 °C using a controlled atmosphere tube furnace, then detached by peeling away the filter paper. XRD was performed using an X-ray tube with a wavelength output of Cu-K_α (λ = 0.154056 nm).

Acknowledgements

This work was supported by the strategic research funds from the Natural Sciences and Engineering Research Council of Canada (NSERC).

References

1 M. J. Yacaman, J. A. Ascencio, H. B. Liu and J. Gardea-Torresdey, *J. Vac. Sci. Technol., B: Microelectron. Nanometer Struct.–Process., Meas., Phenom.*, 2001, **19**, 1091–1103.
2 A. Desireddy, B. E. Conn, J. Guo, B. Yoon, R. N. Barnett, B. M. Monahan, K. Kirschbaum, W. P. Griffith, R. L. Whetten, U. Landman and T. P. Bigionil, *Nature*, 2013, **501**, 399–402.
3 L. H. Liang, C. M. Shen, S. X. Du, W. M. Liu, X. C. Xie and H. J. Gao, *Phys. Rev. B: Condens. Matter Mater. Phys.*, 2004, **70**, 205419.
4 M. Zhao and Q. Jiang, *Key Eng. Mater.*, 2010, **444**, 189–217.
5 X. Liu, A. Wang, X. Yang, T. Zhang, C.-Y. Mou, D.-S. Su and J. Li, *Chem. Mater.*, 2009, **21**, 410–418.
6 J. Sun, D. Ma, H. Zhang, X. Liu, X. Han, X. Bao, G. Weinberg, N. Pfander and D. Su, *J. Am. Ceram. Soc.*, 2006, **128**, 15756–15764.
7 J.-H. Shim, B.-J. Lee and Y. W. Cho, *Surf. Sci.*, 2002, **512**, 262–268.
8 G. Guisbiers, G. Abudukelimu, F. Clement and M. Wautelet, *J. Comput. Theor. Nanosci.*, 2007, **4**(2), 309–315.
9 X. Chen and H. J. Schluesener, *Toxicol. Lett.*, 2007, **176**, 1–12.
10 C. Liu, X. Yang, H. Yuan, Z. Zhou and D. Xiao, *Sensors*, 2007, **7**, 708–718.
11 A. Kumar, P. K. Vemula, P. M. Ajayan and G. John, *Nat. Mater.*, 2008, **7**, 236–241.
12 A. Murugadoss and A. Chattopadhyay, *Nanotechnology*, 2008, **19**, 015603.
13 I.-K. Shim, Y. I. Lee, K. J. Lee and J. Joung, *Mater. Chem. Phys.*, 2008, **110**, 316–321.
14 L. Zhao, K. L. Kelly and G. C. Schatz, *J. Phys. Chem. B*, 2003, **107**, 7343.
15 S. Panigrahi, S. Praharaj, S. Basu, S. K. Ghosh, S. Jana, S. Pande, T. Vo-Dinh, H. Jiang and T. Pal, *J. Phys. Chem. B*, 2006, **110**, 13436.
16 J. L. Speshock, R. C. Murdock, L. K. Braydich-Stolle, A. M. Schrand and S. M. Hussain, *J. Nanobiotechnol.*, 2010, **8**, 19.
17 J. L. Elechiguerra, J. L. Burt, J. R. Morones, A. C. Bragado, X. Gao, H. H. Lara and M. J. Yacaman, *J. Nanobiotechnol.*, 2005, **3**, 6.
18 F. Zhang, X. Wu, Y. Chen and H. Lin, *Fibers Polym.*, 2009, **10**(4), 496.
19 N. Pradhan, A. Pal and T. Pal, *Colloids Surf., A*, 2002, **196**, 247.
20 H. Cai, Y. Xu, N. Zhu, P. He and Y. Fang, *Analyst*, 2002, **127**, 803.
21 A. R. Tao, S. Habas and P. Yang, *Small*, 2008, **4**(3), 310.
22 Y. Sun and Y. Xia, *Science*, 2002, **298**, 2176.
23 B. Wiley, Y. Sun and Y. Xia, *Acc. Chem. Res.*, 2007, **40**, 1067.
24 J. L. Elechiguerra, J. Reyes-Gasga and M. J. Yacaman, *J. Mater. Chem.*, 2006, **16**, 3906.
25 Y. Sun, B. Mayers, T. Herricks and Y. Xia, *Nano Lett.*, 2003, **3**(7), 955.
26 A. M. Leach, M. McDowell and K. Gall, *Adv. Funct. Mater.*, 2007, **17**, 43.
27 J. Y. Lee, S. T. Connor, Y. Cui and P. Peumans, *Nano Lett.*, 2008, **8**(2), 689.
28 R. Gunawidjaja, C. Jiang, S. Peleshanko, M. Ornatska, S. Singamaneni and V. V. Tsukruk, *Adv. Funct. Mater.*, 2006, **16**, 2024.
29 P. Peng, H. Huang, A. Hu, A. P. Gerlicha and Y. N. Zhou, *J. Mater. Chem.*, 2012, **22**, 15495.
30 T. Y. Kim, Y. W. Kim, H. S. Lee, H. Kim, W. S. Yang and K. S. Suh, *Adv. Funct. Mater.*, 2013, **23**, 1250.
31 J. Feng, X. Ma, H. Mao, B. Liu and X. Zhao, *J. Mater. Res.*, 2011, **26**(21), 2691.
32 H. H. Khaligh and I. A. Goldthorpe, *Nanoscale Res. Lett.*, 2013, **8**, 235.
33 X. Zhang, X. Yan, J. Chen and J. Zhao, *Carbon*, 2014, **69**, 437.
34 J. P. Farney, G. W. Kammlott and T. E. Graedel, *Corros. Sci.*, 1985, **25**(2), 133.
35 J. L. Elechiguerra, L. Larios-Lopez, C. Liu, D. Garcia-Gutierrez, A. Camacho-Bragado and M. J. Yacaman, *Chem. Mater.*, 2005, **14**, 6042.
36 E. Marzbanrad, A. Hu, B. Zhao and Y. Zhou, *J. Phys. Chem. C*, 2013, **117**, 16665.
37 R. Jin, Y. W. Cao, C. A. Mirkin, K. L. Kelly, G. C. Schatz and J. G. Zheng, *Science*, 2001, **294**, 1901.

38 M. Maillard, S. Giorgio and M.-P. Pileni, *Adv. Mater.*, 2002, **14**(15), 1084.
39 I. Pastoriza-Santos and L. M. Liz-Marzán, *Nano Lett.*, 2002, **2**(8), 903.
40 Y. Sun, B. Mayers and Y. Xia, *Nano Lett.*, 2003, **3**(5), 675.
41 W. Humphrey, A. Dalke and K. Schulten, *J. Mol. Graphics*, 1996, **14**(1), 33.
42 J. Li, *Modell. Simul. Mater. Sci. Eng.*, 2003, **11**, 173.
43 M. S. Daw and M. I. Baskes, *Phys. Rev. Lett.*, 1983, **50**(17), 1285.
44 M. S. Daw and M. I. Baskes, *Phys. Rev. B: Condens. Matter Mater. Phys.*, 1984, **29**(12), 6443.
45 S. M. Foiles, M. I. Baskes and M. S. Daw, *Phys. Rev. B: Condens. Matter Mater. Phys.*, 1986, **33**(12), 7983.
46 W. G. Hoover, *Phys. Rev. A: At., Mol., Opt. Phys.*, 1985, **31**(3), 1695.
47 J. M. Hail, *Molecular dynamics simulation: Elementary Methods*, John Wiley & Sons, 1992.
48 G. J. Ackland and A. P. Jones, *Phys. Rev. B: Condens. Matter Mater. Phys.*, 2006, **73**(5), 054104.
49 Y. G. Sun, B. Gates, B. Mayers and Y. N. Xia, *Nano Lett.*, 2002, **2**(2), 165.
50 Y. G. Sun and Y. N. Xia, *Adv. Mater.*, 2002, **14**(11), 833.
51 P. Peng, A. M. Hu, H. Huang, A. P. Gerlich, B. X. Zhao and Y. N. Zhou, *J. Mater. Chem.*, 2012, **22**(26), 12997.
52 P. Peng, H. Huang, A. M. Hu, A. P. Gerlich and Y. N. Zhou, *J. Mater. Chem.*, 2012, **22**(31), 15495.
53 B. M. Amoli, E. Marzbanrad, A. Hu, Y. N. Zhou and B. Zhao, *Macromol. Mater. Eng.*, 2014, **229**, 739.

Published on 31 October 2014. Downloaded on 27/02/2015 20:24:12.

 This journal is © the Owner Societies 2015